Numerical simulations investigating the isotope effect in the plasma sheath of negative ion sources for fusion NBI

Grace Kirk*, Max Lindqvist, Dirk Wünderlich, Serhiy Mochalskyy, and Ursel Fantz

Max-Planck-Institut für Plasmaphysik, Garching, Germany
*grace.kirk@ipp.mpg.de

1 Introduction

The ITER tokamak requires two Neutral Beam Injectors (NBIs) capable of supplying 16.5 MW per beamline with particle energies of 1 MeV in hydrogen (H) and 0.87 MeV in deuterium (D) for current drive and plasma heating [1]. Negative Neutral Beam Injectors (NNBI) are needed because negative ions can be neutralized efficiently (approximately 60%) at these high energies, whereas efficient neutralization of positive ions becomes impossible [2]. The negative ion source, which forms the front end of the NNBI, must deliver: high extracted negative ion current density (H^-: 329 A/m^2, D^-: 286 A/m^2), low co-extracted electron current density (co-extracted electron-to-ion ratio ≤ 1), high beam uniformity (90%), and low single-beamlet divergence (≤ 7 mrad) for long pulses in both hydrogen and deuterium (3600 s for D, hundreds of seconds for H) [3]. Reaching these requirements is difficult as pulse performance is limited by excessive heating of the extraction system, where co-extracted electrons are deflected by permanent magnets [4]. This is particularly problematic in deuterium operation, compared to hydrogen, where the co-extracted electron current is higher and grows more rapidly over time [4].

2 Methodology

Negative ions are created through two mechanisms, as illustrated in Fig. 1A: volume production via dissociative electron attachment, and surface production through surface negative ionization [5]. Because ITER requires a filling pressure of 0.3 Pa or less, surface production is dominant, whereby cesium is deposited onto the plasma grid to lower its Work Function (WF), enabling it to act as a conversion surface from which atoms and positive ions can pick up additional electrons [4]. The estimated negative ion flux off the plasma grid surface within the ELISE negative ion source (Fig. 1B) for a WF of 1.6 eV is approximately 550 A/m^2 [6]. This flux from the plasma grid builds a localized negative space charge within the plasma-wall sheath which can form a potential well known as a virtual cathode (VC). However, this virtual cathode reduces the flux of negative ions towards the bulk plasma. This occurs because the charge balance at the wall requires that the total negative current density (electrons and negative ions) equal the positive ion current density. When the surface produced negative ion current density from the plasma grid surpasses this limit, a virtual cathode forms, reflecting back negative ions that lack sufficiently high energies [7].

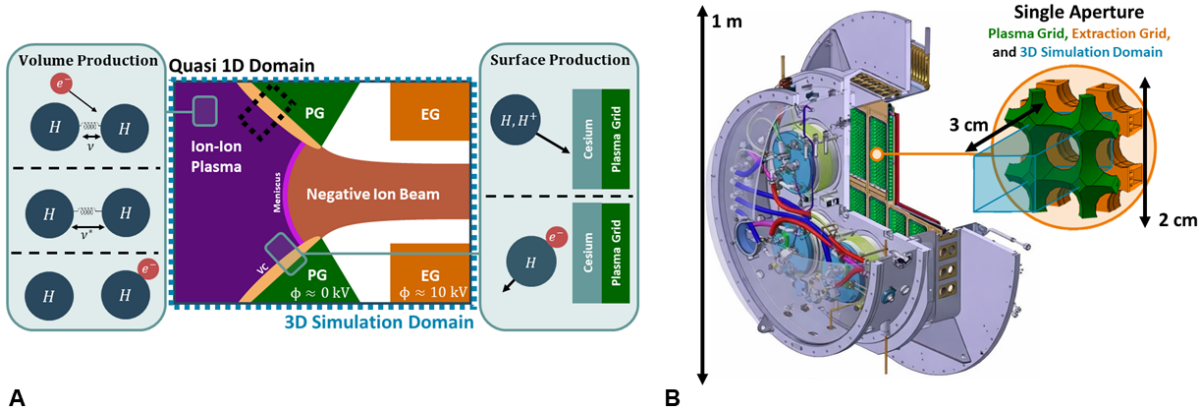

Fig. 1. A) Illustration of near aperture physics showing: representative quasi 1D domain highlighted in black, 3D domain highlighted in blue, with the plasma grid (PG) in green and extraction grid (EG) in orange, meniscus in pink, virtual cathode in light orange, and negative ion creation via volume (far left) and surface production (far right) in the region of beam extraction. B) (left) Schematic of the Radio Frequency (RF) driven ELISE negative ion source [8]. (right) Single aperture of plasma and extraction grids highlighting the 3D simulation domain.

In a negative ion source for fusion (such as the one for ELISE Fig. 1B [8]), negative ions are extracted by a potential difference of approximately 10 kV applied between the plasma and extraction grid (Fig. 1A) [4]. This potential penetrates into the plasma, forming a distinct boundary, the meniscus, between the quasineutral bulk plasma and the negative ion beam (Fig. 1A). The shape and position of the meniscus have a significant influence on the ion optics of the extracted beam as well as on co-extraction of electrons [9].

These interactions, the virtual cathode and meniscus, between the quasineutral plasma and the extraction region dictate how the negative ion beam is formed. Experimental diagnostic techniques cannot access the plasma in this region, preventing direct insight into beam formation. Simulations offer valuable insight towards improving the extraction and acceleration of negative ions. By using a 3D kinetic code, the plasma sheath of this region may be fully resolved, providing a model of the plasma-wall interface under the effects of surface-produced negative ions [4].

The Orsay Negative Ion eXtraction code (ONIX) models negative ion creation, transport, and extraction within the vicinity of an aperture of a negative ion source, using the Particle-in-Cell Monte Carlo Collisions (PIC-MCC) method in 3D3V for both hydrogen and deuterium plasmas [10], [11], [12]. Simulations typically include one aperture (approximately $12\,\mathrm{cm}^3$ per aperture) at plasma parameters representative of experimental conditions (see Table 1) with magnetic and electric fields at full scale. Resolving the Debye length, λ_D, inverse plasma frequency, and satisfying the Courant–Friedrichs–Lewy (CFL) condition makes these simulations extremely computationally demanding. The code is therefore highly parallelized using the Message Passing Interface (MPI), enabling full-scale simulations that require up to one million core-hours on High-Performance Computing (HPC) clusters.

Table 1. Bulk plasma parameters for the computational model, representative of experimental conditions in the ELISE negative ion source. Note that in the experiment H and D plasma parameters differ [4].

Species	n [m^{-3}]	T [eV]
Electrons (e^-)	4.0×10^{16}	2.0
Negative ions (H^-/D^-)	2.0×10^{16}	0.6
Monoatomic positive ions (H^+/D^+)	2.4×10^{16}	0.8
Diatomic positive ions ($H_2{}^+/D_2{}^+$)	2.4×10^{16}	0.1
Triatomic positive ions ($H_3{}^+/D_3{}^+$)	1.2×10^{16}	0.1

Within the model, positive species are injected at set temperatures and regulated by a Proportional-Integral-Derivative (PID) controller until the desired densities (Table 1) are reached, while the electron flux maintains quasineutrality [11]. As shown in Table 1, the negative ion density should approximately equal the positive ion density; however, the code has thus far been unable to reproduce self-consistently the negative ion density through surface and volume production processes. The virtual cathode is hypothesized to be key in inhibiting this reproduction. The motivation for the present work is therefore to investigate virtual cathode formation in the plasma sheaths as a potential limiting factor in achieving the desired negative ion densities in the model for both hydrogen and deuterium plasmas.

3 Results

Parametric scans were performed to assess plasma sheath behavior, with particular focus on virtual cathode formation, under the bulk plasma conditions given in Table 1, for both hydrogen and deuterium. A quasi-1D domain representative of the plasma sheath at the plasma grid was adopted, as highlighted by the black box in Fig. 1A. This reduced dimensionality allows the sheath structure to be studied across numerous parametric scans that would be impractical in 3D. The full domain spans $80\lambda_D$, with further details of the boundary conditions and domain illustrated in Fig. 2. Because of the mass difference, to accurately reproduce equivalent H/D plasma densities at a fixed injection temperature, emission rates were scaled by the thermal velocity ratio, giving $\Gamma_{\mathrm{H}^-} = \sqrt{2}\,\Gamma_{\mathrm{D}^-}$. The resulting emission rates were $\Gamma_{\mathrm{H}^-} = 550\,\mathrm{A/m}^2$ and $\Gamma_{\mathrm{D}^-} = 390\,\mathrm{A/m}^2$ to isolate the isotopic mass effect.

Within the plasma, the different charged species (H_x^+/D_x^+, $H^-/D^-, e^-$) drive virtual cathode behavior. An objective of this work was to quantify each species impact on the virtual cathode and therefore the resulting bulk negative ion densities. The species temperatures and negative ion emission rates were varied ($0.1 \leq T_{sp} \leq 5\,\mathrm{eV}$ and $18 \leq \Gamma_{\mathrm{H}^-/\mathrm{D}^-} \leq 1000\,\mathrm{A/m}^2$), and virtual cathode behavior was then quantified by its depth, $\Delta\phi$. Fig. 2 shows an example result of plasma potential across the domain and how it varies between H/D plasmas for increasing electron temperature ($T_e = 0.5, 2, 5eV$).

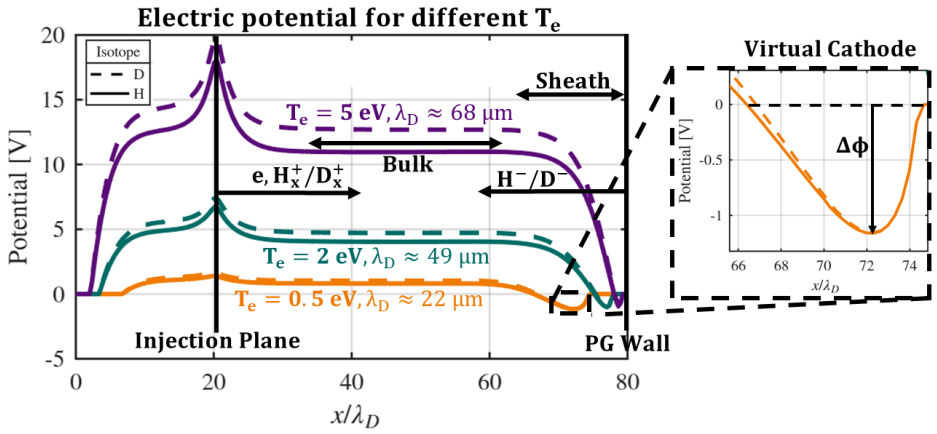

Fig. 2. Example scan showing the effect of electron temperature on plasma potential across a quasi-1D domain of $80\lambda_D$, for hydrogen and deuterium. Positive ions and electrons are injected at the left boundary; negative ions are emitted at the right (plasma grid). The domain is normalized by the debye length, and the virtual cathode depth is marked to the right.

Fig. 2 confirms the validity of the model: the bulk plasma potential, ϕ_{Plasma}, is consistently higher in deuterium and increases with electron temperature, both of which are in agreement with fundamental plasma physics. Ambipolar diffusion establishes the plasma potential, and a heavier, hotter plasma requires a higher potential to balance ion and electron fluxes to the wall and maintain quasineutrality. Similar trends in the simulated plasma potentials in H and D are found and agree with the simplified Stangeby analytical expression, $(\phi_{Plasma} = -\frac{T_e}{2} ln\left(\frac{2\pi m_e}{m_i}\right))$ [13].

The isotopic dependence was studied by varying the emission rates in H and D. Fig. 3A shows virtual cathode depth as a function of increasing negative ion temperature for different flux rates in H (line with square markers) and D (line with circle markers). At a given temperature with equal fluxes ($\Gamma_{\mathrm{H}^-} = \Gamma_{\mathrm{D}^-}$), deuterium consistently develops a deeper virtual cathode. This arises because, at a fixed $T_{\mathrm{H}^-/\mathrm{D}^-}$, the lower thermal velocity of D^- leads to a higher accumulated density near the emitting surface. To match negative ion densities, thermal velocity-scaled fluxes are applied instead (comparing the solid teal line with squares to teal line with circles). The virtual cathode in deuterium becomes very slightly shallower as a consequence of enhanced D^- transport driven by the higher bulk plasma potential. While this slight variation between the two isotopes remains, once the emission rates are scaled by their differing thermal velocities, no significant difference in virtual cathode depth is found between hydrogen and deuterium plasmas, as seen across all parametric scans.

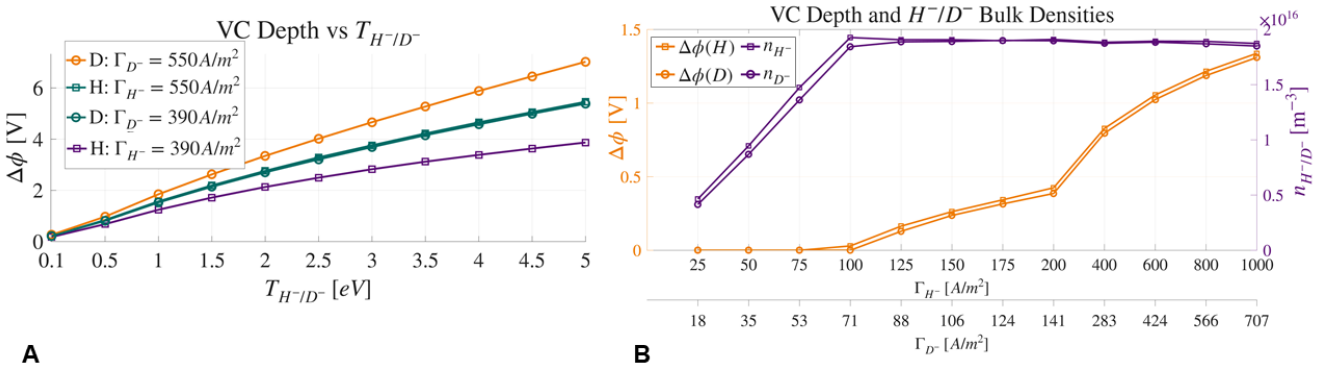

Fig. 3. A) Effect of increasing negative ion temperature $0.1 \leq T_{\mathrm{H}^-/\mathrm{D}^-} \leq 5$ eV on virtual cathode depth under different emission rates (390 and 550 $\mathrm{A/m^2}$) for H/D. Varying the emission rates by a factor of $\sqrt{2}$ allowed the mass effect to be fully isolated. B) Impact of increasing emission rate $25 \leq \Gamma_{\mathrm{H}^-} \leq 1000$ $\mathrm{A/m^2}$ and $18 \leq \Gamma_{\mathrm{D}^-} \leq 707$ $\mathrm{A/m^2}$ for fixed $T_{\mathrm{H}^-/\mathrm{D}^-} = 0.6$ eV on virtual cathode depth (left axis, orange line) and negative ion density (right axis, purple line), taken at the quasineutral bulk.

From the parametric scans it is clear that at a fixed plasma density, increasing the electron temperature from $0.5 \leq T_e \leq 5$ reduces the virtual cathode depth by approximately 20% (Fig. 2), while varying positive ion temper-

ature $0.1 \leq T_{H_x^+/D_x^+} \leq 5$ eV has no effect (not shown). Higher electron temperatures raise the plasma potential, thereby providing a stronger acceleration of H^-/D^- towards the bulk via the plasma sheath, whereas positive ions have no influence on this process. In contrast, variations in negative ion emission rate or temperature produce an order-of-magnitude increase in virtual cathode depth (Fig. 3A teal line, Fig. 3B orange line).

Increasing either Γ_{H^-/D^-} or T_{H^-/D^-} raises the negative ion current density and deepens the virtual cathode. However, as seen in Fig. 3A/B, increasing T_{H^-/D^-} at a fixed $\Gamma_{H^-/D^-} = 550/390$ A/m^2 produces a significantly deeper virtual cathode than increasing Γ_{H^-/D^-} at a fixed $T_{H^-/D^-} = 0.6$ eV, as the current scales more strongly with temperature than emission rate. A further distinction between the two cases is the bulk negative ion density: when Γ_{H^-/D^-} is increased, the bulk density saturates once a virtual cathode forms while as T_{H^-/D^-} is increased, the bulk density continues to rise even in the presence of a virtual cathode. This has an important implication, indicating that further studies in 3D with raised negative ion temperatures would be worthwhile.

4 Conclusions

The overall goal of full-scale single-aperture modeling is to simulate the near-aperture physics of the ion source as self-consistently as possible, capturing behavior that would otherwise remain inaccessible to experimental diagnostics. Understanding negative ion sheaths is an important step towards this goal, as virtual cathodes within these sheaths arise from surface production and limit the transport to the plasma and therefore the bulk negative ion density. The parametric scans in a reduced domain demonstrate that negative ion emission rate and temperature are the primary drivers of virtual cathode behavior, while electron temperature reduces virtual cathode depth and positive ion temperature has no effect. When emission rates are scaled by the thermal velocity ratio such that the mass dependence is isolated, no isotope effect is observed in virtual cathode behavior. These findings provide a foundation for the more computationally expensive full 3D investigations, and future work will focus on further improving the self-consistent creation of negative ions. Full 3D simulations will then be used to investigate isotope-dependent meniscus behavior, using experiment parameters in hydrogen and deuterium plasmas to evaluate the isotope effect consistently.

References

1. International Atomic Energy Agency. *ITER Technical Basis*. Number 24 in ITER EDA Documentation Series. International Atomic Energy Agency, Vienna, 2002.
2. K. Berkner, R. Pyle, and J. Stearns. Intense, mixed-energy hydrogen beams for CTR injection. *Nuclear Fusion*, 15(2):249, 1975.
3. Alberto Loarte et al. The new ITER baseline, research plan and open R&D issues. *Plasma Physics and Controlled Fusion*, 67(6):065023, 2025.
4. U. Fantz et al. Negative hydrogen ion sources for fusion: From plasma generation to beam properties. *Frontiers in Physics*, 9:709651, 2021.
5. Marthe Bacal, Mamiko Sasao, and Motoi Wada. Negative ion sources. *Journal of Applied Physics*, 129(22), 2021.
6. M. Seidl et al. Negative surface ionization of hydrogen atoms and molecules. *Journal of Applied Physics*, 79(6):2896–2901, 1996.
7. J. W. Luginsland, Y. Y. Lau, and R. M. Gilgenbach. Two-dimensional Child-Langmuir law. *Physical Review Letters*, 77(22):4668, 1996.
8. U. Fantz et al. *Nuclear Fusion*, 57:116007, 2017.
9. Max Lindqvist. *Insights into the plasma and beam physics close to the extraction surface in H^-/D^- sources for fusion based on 3D-PIC MCC modeling*. Dr. rer. nat. dissertation, Universität Augsburg, Augsburg, Germany, 2024.
10. Serhiy Mochalskyy et al. 3D modelling of negative ion extraction from a negative ion source. *Nuclear Fusion*, 56(10):106025, 2016.
11. M. Lindqvist et al. Particle injection methods in 3-D-PIC MCC simulations applied to plasma grid biasing. *Physics of Plasmas*, 31(3), 2024.
12. Charles K. Birdsall. Particle-in-cell charged-particle simulations, plus Monte Carlo collisions with neutral atoms, PIC-MCC. *IEEE Transactions on Plasma Science*, 19(2):65–85, 1991.
13. P. C. Stangeby. Plasma sheath transmission factors for tokamak edge plasmas. *Physics of Fluids*, 27(3):682–690, 1984.